JOURNAL OF AIRCRAFT
Vol. 47, No. 4, July–August 2010

Engineering Notes

Numerical Simulation of Rotor–Fuselage–Cylinder Interaction in Forward Flight

Yihua Cao,* Ming Zhao,† and Li Hu‡
Beijing University of Aeronautics and Astronautics, 100191 Beijing, People's Republic of China

DOI: 10.2514/1.45160

Introduction

BECAUSE fuselage could have a significant effect on the overall performance of the rotorcraft, the rotor–fuselage interaction has been analyzed [1–4]. Actuator disc method is widely implemented to determine the time-averaged effect of the rotor on the fuselage. A comprehensive introduction of actuator disc method can be found in the work of Le Chuiton [5]. This method will not give a time-accurate solution at individual blades; however, it reduces the cost in some extent. Actuator disc method mentioned as momentum source method has been presented by Rajagopalan [6].

Detailed CFD modeling of the individual blades has been investigated. For example, unsteady flowfield and airloads on rotor have been computed by Ahmad and Duque [7] with the application of overset grid technology. Combined with Kirchhoff acoustics prediction scheme [8], computed results for far-field noise are compared with experimental data by Duque et al. [9]. Overset grid technology has also been extended for full aircraft to investigate the impact of rotor wake system on the flowfield [10].

Other aspects of helicopter aerodynamics have also been investigated. For example, helicopter slung load aerodynamics has been studied by Theron et al. [11].

Although considerable research has been devoted to the capture of flowfield details, rather less attention has been paid to the interaction between the fuselage and bluff bodies, whereas unsteady separated flow from bluff bodies is a very common existence and of great significance in practice. It causes fluctuating drag and lateral force to the body and is a major source of flow-induced structural vibration and noise [12], and there has been growing interest in fluid-structure interactions of cylinder [13,14].

Some flowfield characteristics of the ROBIN model [15] are obtained, and the accuracy is quantitatively validated by comparing the results with experimental data and reference. The novelty lies in the consideration of adjunctive cylinders for the MI-171 helicopter; however, the deformation of cylinders is not under consideration. This attempt provides a method devoted to optimization design in case there is any requirement to suspend an object beneath fuselage.

Received 28 April 2009; revision received 19 January 2010; accepted for publication 1 February 2010.

*Professor, School of Aeronautic Science and Engineering; yihuacs@yahoo.com.cn (Corresponding Author).
†Ph.D. Candidate, School of Aeronautic Science and Engineering.
‡M.S. Candidate, School of Aeronautic Science and Engineering.

Grid and Calculation Conditions

Multiblock structured grid is adopted. The mesh must be constructed with an interface corresponding to the surface swept by the blades. For the ROBIN model, the mesh has about 1.8 million nodes distributed in 42 blocks, and there are about 2.5 million nodes in the mesh generated for MI-171. The distance from the center of the rotor to the far-field boundary is about $10R$ (R denotes the rotor radius). The mesh of the ROBIN model is demonstrated in Fig. 1. The topology is similar with that in [1].

The surface mesh for the MI-171 configuration, which has an attachment composed of two cylinders, is shown in Fig. 2. The diameter of the circular cylinder is 0.3 m, and the span is 1.2 m. The dimensions of the square cylinder are as follows: length (x direction) $L = 2.1$ m, width (y direction) $W = 0.6$ m, and height (z direction) $H = 0.78$ m.

Figures 1 and 2 also illustrate the directions of the coordinates. Z axis points upward for both cases. For MI-171, the X axis points to the nose, and the X axis points to the tail for the ROBIN model. The origin for MI-171 is settled at the center of front landing gear, in contrast to ROBIN, for which the origin is overlapped with the hub center.

The parameters of the ROBIN model are as follows. For an isolated fuselage, the forward-flight velocity $V = 21.2$ m/s. For the rotor–fuselage case, the parameters are presented in Table 1. Parameters of isolated fuselage and rotor–fuselage case are cited from [1,15], respectively.

There are few trim data for MI-171 helicopter suspending cylinders, since it is an imaginary model to analyze the interactions among the components. Calculation conditions are the same as the case without cylinders. The calculation conditions for the MI-171 helicopter are presented in Table 2.

The surface is treated as a no-slip wall for viscous simulation. Outer boundaries are known as the velocity inlet. Velocity is calculated based on forward-flight velocity and angle of attack.

Governing Equations, Algorithm, and Actuator Disc Model

The governing equations used in this work are the incompressible three-dimensional Navier–Stokes equations.

Continuity equation:

$$\frac{\partial U_i}{\partial x_i} = 0 \tag{1}$$

Momentum equation:

$$\frac{\partial U_i}{\partial t} + U_j \frac{\partial U_i}{\partial x_j} = -\frac{1}{\rho}\frac{\partial P}{\partial x_i} + \nu \frac{\partial^2 U_i}{\partial x_j \partial x_j} + \frac{1}{\rho}\frac{\partial(-\rho\overline{u_i' u_j'})}{\partial x_j} \tag{2}$$

where U_i denotes the velocity tensor, and $-\rho\overline{u_i' u_j'}$ denotes the Reynolds stress.

Many turbulence models have been established to relate the fluctuating value and the mean value, so that the governing equations can be solved [16]. The Spalart–Allmaras model [17] adopted here is a one-equation turbulence model.

Finite volume method is used to discretize the differential equations, and the convective terms are discretized with third-order MUSCL scheme [18]. SIMPLE algorithm [19] is implemented to solve the three-dimensional viscous incompressible Reynolds-averaged Navier–Stokes (RANS) equations.

The rotating blades are replaced by an infinitely thin disk across which the momentum and energy of the flow are increased by

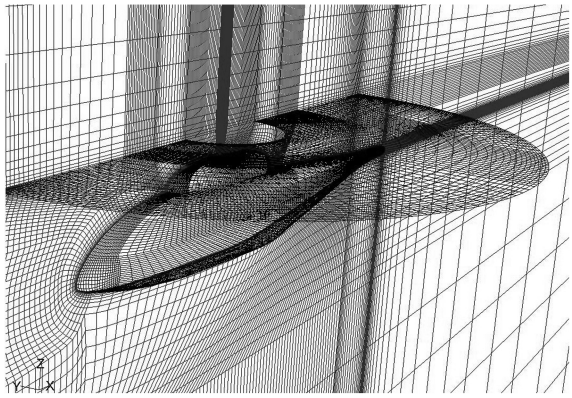

Fig. 1 ROBIN configuration. Symmetry plane, actuator plane, and fuselage wall.

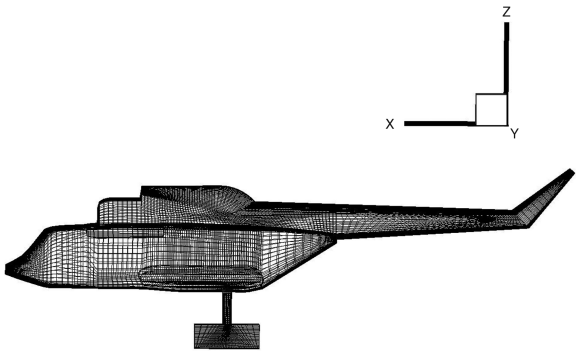

Fig. 2 Surface mesh for the MI-171 with cylinders.

quantities equivalent to the work and energy supplied by the rotor to the flow [1].

Calculation Results and Analysis Isolated Fuselage and Actuator Disc Model

For the isolated fuselage of ROBIN model, the pressure coefficient distribution along the top centerline derived from present computation is demonstrated by the solid line in Fig. 3, and the hollow squares indicate the result of FLU3M computation [1]. Coincidence of the results validates the accuracy of this methodology.

Uniform actuator disc is applied for the ROBIN model. Uniform distribution of the rotor thrust is equivalent to a constant pressure jump according to uniform actuator disk theory:

Table 1 Parameters for rotor–fuselage case

Parameters	Values
Forward-flight velocity V	9.88472 m/s
Rotational speed ω	125.6 rad/s
Rotor diameter D	3.148 m
Rotor thrust coefficient C_T	0.00502

Table 2 Calculation conditions for MI-171 helicopter

Parameters	Values
Flying altitude H	4000 m
Advance ratio μ	0.05
Rotor diameter D	21.3 m
Rotational speed ω	20.096 rad/s
Angle of attack α	-5°

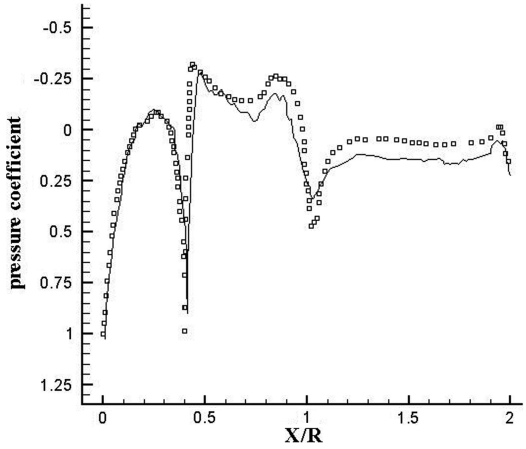

Fig. 3 Pressure coefficient distribution along the top centerline.

$$\Delta p_R = C_T \cdot \rho_\infty \cdot \left(\omega_R \cdot \frac{D_R}{2}\right)^2 = 240\ \mathrm{N \cdot m^{-2}} \tag{3}$$

where subscript R denotes ROBIN model.

The pressure distributions on selected sections are displayed in Fig. 4. The solid lines indicate the pressure distributions obtained from present computation, and the hollow squares indicate the experimental data [15]. They coincide with each other well. The results are presented mainly to make sure the methodology is reliable.

Fuselage–Cylinder Interaction

The calculation for the case including cylinders is unsteady. The pressure distributions of MI-171 fuselage surface at $t = 100$ s are presented in Fig. 5. The pressure indicated in the legend is relative, and the reference value is 61,640 Pa, and so are the pressure values in Fig. 6.

It could be observed that pressure peak values appear at the cylinders, so it might be concluded that the cylinders carry a considerable backward load.

Vortex streets observed in flows past bluff bodies appear due to instabilities in the wake and shear layers. It is mutual interaction between the two shear layers that causes the onset of vortex shedding [13].

Streamlines and pressure distributions around the circular cylinder at forward-flight velocity $V = 10.7$ m/s are shown in Fig. 6. Temporal evolution of the wake flow over one time period of vortex shedding is demonstrated as unsteady solutions are achieved.

Wake vortices shedding alternatively from the right and left sides of the cylinder surface are demonstrated in Fig. 6. Vortex-shedding frequency could be evaluated approximately. An attempt to interpret the pattern has been carried out in [20]. According to that paper, there is a closed cavity behind the circular cylinder during the starting-up process, and once vortex shedding begins, instantaneous alleyways of fluid penetrate the cavity as shown in Fig. 7a. Similar alleyways could be somewhat observed in Fig. 7b, which sketches the instantaneous streamlines behind circular cylinder at $t=$ 100.0475 s.

The elasticity of the cylinder has been ignored, so the structure is completely rigid. Consequently, some features of vortex-induced vibration (e.g., lock-in phenomenon) might not be detected; however, it still has significance in engineering, since the structure design could evade induced vibration. Vortex shedding most commonly induces oscillations in a direction transverse to that of the stream at flow speeds where the vortex-shedding frequency coincides with the body oscillation frequency. Crossflow amplitude versus reduced velocity for a circular cylinder has been investigated [21]. According to the conclusion proposed by Bearman [21], the amplitude appears to augment at the reduced velocity $Ur = 5 \sim 7.4$ for freely vibrating bluff body as an aspect of lock-in phenomenon.

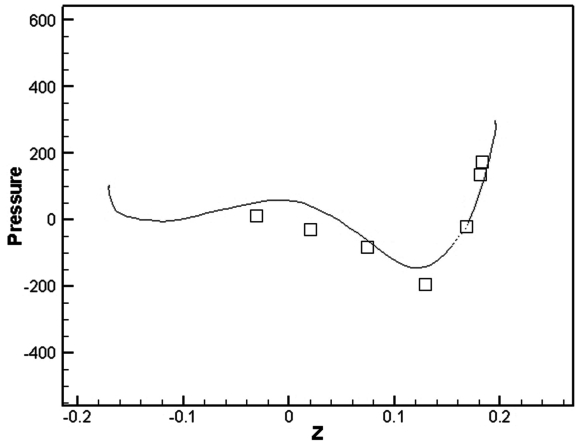

a) x/R=0.307

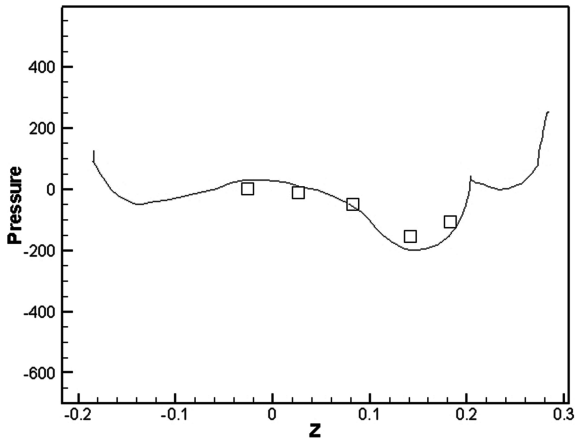

b) x/R=0.467

Fig. 4 Pressure distributions on selected sections.

Reduced velocity is defined as U/ND_C, where N is the body oscillation frequency; D_C is the diameter of the circular cylinder. As the reduced velocity is relevant to the diameter, D_C might be optimized to keep reduced velocity away from the interval of lock-in. Furthermore, D_C is also a crucial factor in determining the body oscillation frequency; therefore it is an optimization process to figure out the radial dimension.

It is known that the flow pattern of the circular cylinder wake varies as Reynolds number Re changes. Figure 8a reveals that there are

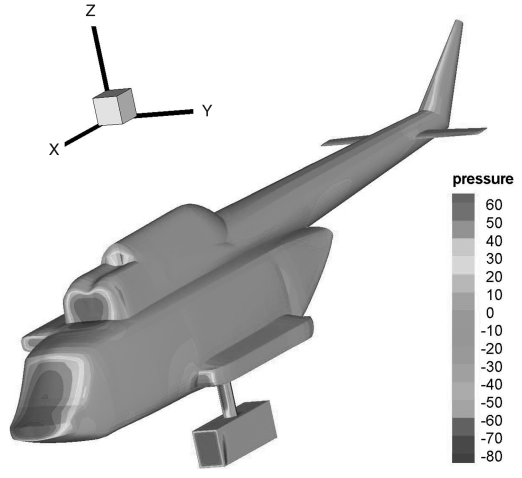

Fig. 5 Pressure distribution of MI-171 fuselage surface (fuselage and cylinders).

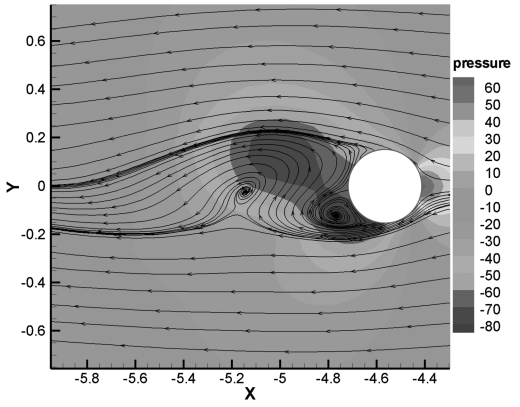

a) t=100.035s

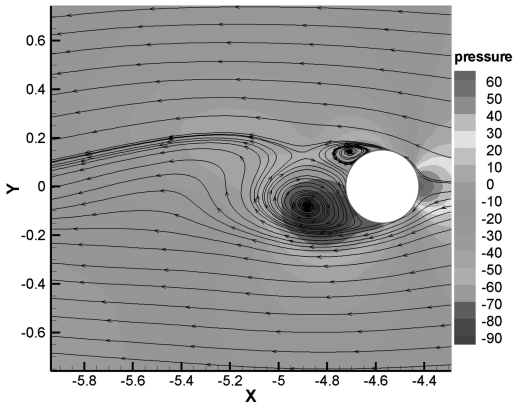

b) t=100.04s

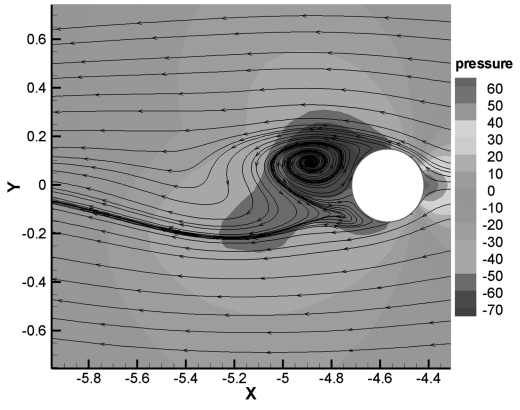

c) t=100.045s

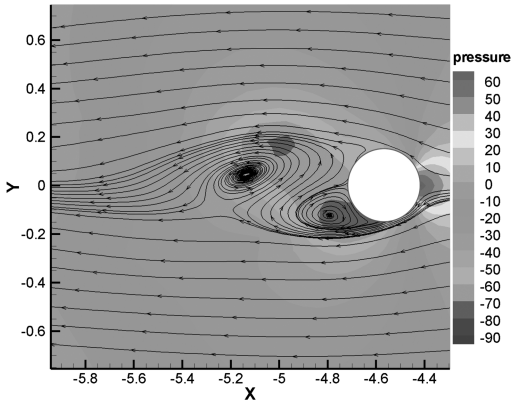

d) t=100.05s

Fig. 6 Streamlines and pressure distribution around circular cylinder.

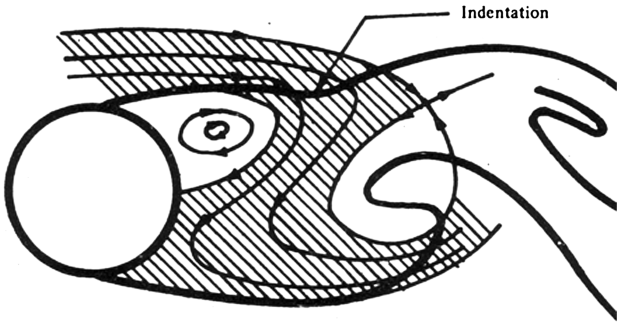

a)

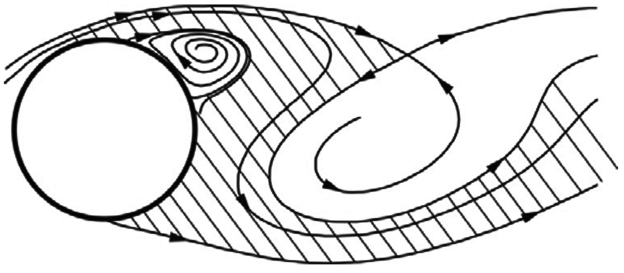

b)

Fig. 7 Illustrations of a) instantaneous streamlines and dye traces behind circular cylinder in [20] and b) instantaneous streamlines behind circular cylinder in present calculation. Crosshatchings indicate instantaneous alleyways.

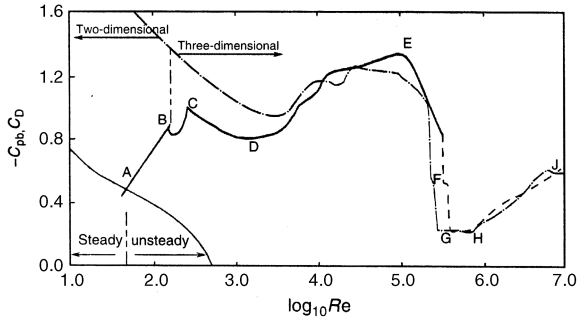

a)

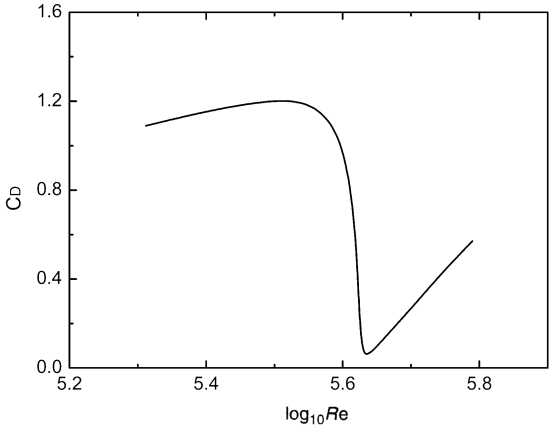

b)

Fig. 8 Plots of a) variation of $-C_{pb}$ (solid and dashed lines) and C_D (dashed-dotted line) in [12] and b) variation of C_D with respect to Reynolds number in present calculation.

different regimes divided by some critical Re marked by $A, B \ldots, J$. In each regime, C_D has corresponding special feature. For $Re < 3\times 10^5$, the boundary layers at both sides are still laminar although the wake and free shear layers have become turbulent. At higher Re the boundary layers at both sides of circular cylinder are turbulent, causing a drastic drop of the C_D (drag crisis). The conclusions mentioned above are obtained for the incompressible flow past a stationary and nominally two-dimensional bluff cylinder [12].

An attempt to find out whether there is a similar feature in present computation is carried out. The range of forward-flight velocity considered here initiates at 10 m/s, where Reynolds number $Re = UD_C/\nu = 2.05 \times 10^5$. The Re dependence of C_D is demonstrated in Fig. 8b.

Drag crisis can also be captured in Fig. 8b. Some distinctions could be found in contrast to Fig. 8a; for instance, the transition after reaching the minimum value seems steeper and the velocity interval around the minimum value appears not as broad as Fig. 8a. In spite of the differences, the tendencies are almost same, and the ranges of C_D coincide with each other well.

The flow beneath fuselage could not be considered uniform, and once the end effect is not negligible, inherently three-dimensional vortex structures must occur that are very different from those observed in the normally two-dimensional midportion of the cylinder [12]. However, according to the regular velocity range of helicopter, the diameter of cylinder might be optimized in engineering to achieve less drag.

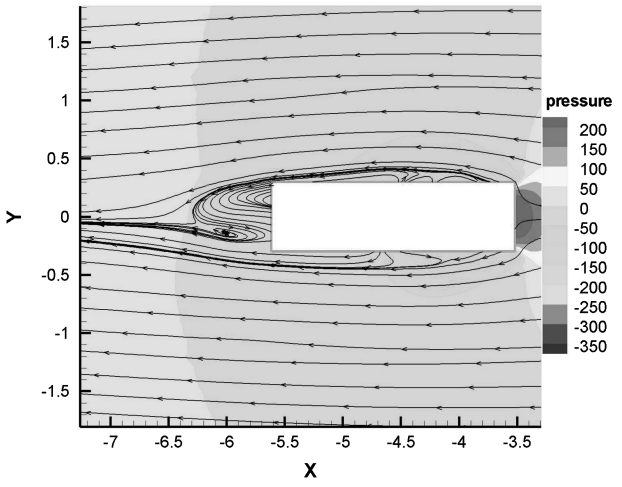

a) t=100.04s, V=20m/s

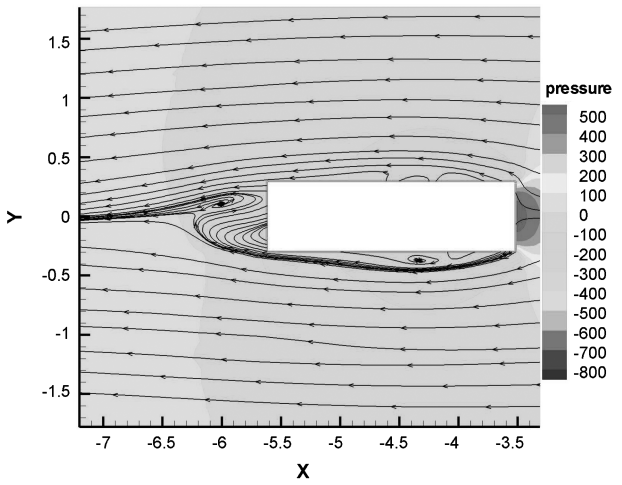

b) t=100.03s, V=30m/s

Fig. 9 Streamlines and pressure distributions around square cylinder.

Figure 9 illustrates the streamlines and pressure distributions around a square cylinder at various velocities. The pressure indicated in the legend is relative, and the reference value is 61,640 Pa. An alleyway could be observed, and the outset of vortex shedding has taken place. The pressure range evidently increases with the augment of forward-flight velocity.

Conclusions

The computational fluid dynamics (CFD) method is adopted to acquire the discrete solution of the helicopter flowfield. Incompressible RANS equations are solved with the application of SIMPLE algorithm. To simulate the time-averaged influence of rotor, the actuator disc model is implemented. A method to capture the vortex-shedding frequency is introduced; in addition, the Reynolds number dependence of circular cylinder drag is also investigated. The conclusions might have some significance in engineering.

References

[1] Bettschart, N., "Rotor Fuselage Interaction: Euler and Navier–Stokes Computations with an Actuator Disc," *55th Annual Forum of the American Helicopter Society* [CD-ROM], AHS International, Alexandria, VA, May 1999.

[2] Chaffin, M. S., and Berry, J. D., "Helicopter Fuselage Aerodynamics Under a Rotor by Navier–Stokes Simulation," *Journal of the American Helicopter Society*, Vol. 42, No. 3, 1997, pp. 235–243. doi:10.4050/JAHS.42.235

[3] Renaud, T., O'Brien, D., Smith, M., and Potsdam, M., "Evaluation of Isolated Fuselage and Rotor-Fuselage Interaction Using CFD," *60th Annual Forum of the American Helicopter Society* [CD-ROM], AHS International, Alexandria, VA, June 2004.

[4] Zori, L., and Rajagopalan, R. G., "Navier–Stokes Calculation of Rotor-Airframe Interaction in Forward Flight," *Journal of the American Helicopter Society*, Vol. 40, No. 2, 1995, pp. 56–67.

[5] Le Chuiton, F., "Actuator Disc Modeling for Helicopter Rotors," *Aerospace Science and Technology*, Vol. 8, No. 4, 2004, pp. 285–297. doi:10.1016/j.ast.2003.10.004

[6] Rajagopalan, R. G., "A Procedure for Rotor Performance, Flowfield and Interference: A Perspective," AIAA Paper 2000-0116, Jan. 2000.

[7] Ahmad, J., and Duque, E., "Helicopter Rotor Blade Computation in Unsteady Flows Using Moving Overset Grids," *Journal of Aircraft*, Vol. 33, No. 1, 1996, pp. 54–60. doi:10.2514/3.46902

[8] Strawn, R. C., Biswas, R., and Lyrintzis, A. S., "Helicopter Noise Predictions using Kirchhoff Methods," *51st American Helicopter Society Annual Forum* [CD-ROM], Alexandria, VA, May 1995.

[9] Duque, E., Strawn, R. C., Ahmad, J., and Biswas, R., "An Overset Grid Navier–Stokes /Kirchhoff-Surface Method for Rotorcraft Aeroacoustic Predictions," AIAA Paper 96-0152, Jan. 1996.

[10] Dimanlig, A., Saberi, H., Meadowcroft, E., Strawn, R., and Bagwhat, M., "Multidisciplinary Modeling of the CH-47 Helicopter with CFD/CSD Coupling and Trim," *DoD HPCMP Users Group Conference*, 2008, pp. 143–149.

[11] Theron, J. N., Gordon, R., Rosen, A., Cicolani, L., Duque, E., and Halsey, R. H., "Simulation of Helicopter Slung Load Aerodynamics: Wind Tunnel Validation of Two Computational Fluid Dynamics Codes," AIAA Paper 2006-3374, June 2006.

[12] Wu, J. Z., Ma, H. Y., and Zhou, M. D., "Separated Vortex Flows," *Vorticity and Vortex Dynamics*, Springer, Berlin, 2006, pp. 323–382.

[13] Yang, J., Preidikman, S., and Balaras, E., "a Strongly Coupled, Embedded-Boundary Method for Fluid-Structure Interactions of Elastically Mounted Rigid Bodies," *Journal of Fluids and Structures*, Vol. 24, 2008, pp. 167–182. doi:10.1016/j.jfluidstructs.2007.08.002

[14] Pratish, P. Patil, and Shaligram Tiwari, "Effect of Blockage Ratio on Wake Transition for Flow Past Square Cylinder," *Fluid Dynamics Research*, Vol. 40, 2008, pp. 753–778. doi:10.1016/j.fluiddyn.2008.04.001

[15] Freeman, C., and Mineck, R., "Fuselage Surface Pressure Measurements of a Helicopter Wind-Tunnel Model with a 3.15-Meter Diameter Single Rotor," NASA TM80051, March 1979.

[16] White, F. M., "Incompressible Turbulent Mean Flow," *Viscous Fluid Flow*, 3rd ed., McGraw–Hill, New York, 2006, pp. 398–498.

[17] Spalart, P. R., and Allmaras, S. R., "a One-Equation Turbulence Model for Aerodynamic Flows," AIAA Paper 1992-439, Jan. 1992.

[18] Van Leer, B., "Towards the Ultimate Conservative Difference Scheme V: A Second Order Sequel to Godunov's Method," *Journal of Computational Physics*, Vol. 32, 1979, pp. 101–136. doi:10.1016/0021-9991(79)90145-1

[19] Pantankar, S. V., and Spalding, D. B., "A Calculation Procedure for Heat, Mass and Momentum Transfer in Three-Dimensional Parabolic Flows," *International Journal of Heat and Mass Transfer*, Vol. 15, 1972, pp. 1787–1806. doi:10.1016/0017-9310(72)90054-3

[20] Perry, A. E., Chong, M. S., and Lim, T. T., "the Vortex-Shedding Process behind Two-Dimensional Bluff Bodies," *Journal of Fluid Mechanics*, Vol. 116, 1982, pp. 77–90. doi:10.1017/S0022112082000378

[21] Bearman, P. W., "Vortex Shedding from Oscillating Bluff Bodies," *Annual Review of Fluid Mechanics*, Vol. 16, 1984, pp. 195–222. doi:10.1146/annurev.fl.16.010184.001211